PCCP

PAPER

Structural phases of adsorption for flexible polymers on nanocylinder surfaces

Jonathan Gross,[ab] Thomas Vogel[cd] and Michael Bachmann[aef]

Cite this: *Phys. Chem. Chem. Phys.*, 2015, **17**, 30702

Received 8th July 2015,
Accepted 5th October 2015

DOI: 10.1039/c5cp03952e

www.rsc.org/pccp

By means of generalized-ensemble Monte Carlo simulations, we investigate the thermodynamic behavior of a flexible, elastic polymer model in the presence of an attractive nanocylinder. We systematically identify the structural phases that are formed by competing monomer–monomer and monomer–substrate interactions. The influence of the relative surface attraction strength on the structural phases in the hyperphase diagram, parameterized by cylinder radius and temperature, is discussed as well. In the limiting case of the infinitely large cylinder radius, our results coincide with previous outcomes of studies of polymer adsorption on planar substrates.

I Introduction

Materials composed of soft and solid condensed matter have been the subject of numerous studies in the past. There are various reasons for this increasing interest, most of which are triggered by the need of advanced technologies for miniature functional devices on nanoscopic and mesoscopic scales such as organic electronic circuits on inorganic substrates and biosensors. However, to achieve systematic progress in understanding the binding mechanisms of polymers at inorganic surfaces in experiments is difficult and costly and theoretical approaches are limited to very simple models. This leaves computer simulations the only flexible tool for thorough studies of models that are capable of reproducing generic features of such hybrid systems. Previous computational studies of lattice and off-lattice polymer adsorption studies on planar surfaces[1–14] and substrates with global and local curvature[15–27] already provided insight into specific properties of different structural phases of adsorbed polymer chains and the analysis of their statistical mechanics.[28]

In this paper, we extend previous studies on adsorption processes of polymers at ultrathin nanowires and their structural hyperphase diagrams[19–21,24] to polymer adsorption at attractive cylindrical substrates[15–18] that resemble, *e.g.*, nanotubes.[22] The major goal is the systematic investigation of the influences of the cylinder radius and the surface attraction strength upon the formation of structural phases for polymers of finite length in a thermal environment. This will result in the construction of the structural hyperphase diagrams of polymer adsorption at cylindrical substrates, parameterized by temperature and cylinder radius, for different surface attraction strengths.

The paper is organized as follows. In Section II, we introduce the model of a flexible, elastic polymer interacting with a cylindrical substrate and describe the details of the simulation method. The canonical statistical analysis of energetic and structural quantities measured in the simulations is performed in Section III. The hyperphase diagrams constructed by means of the results of the thermodynamic analysis are discussed in Section IV. The summary in Section V concludes our study.

II Model and methods

We investigate a generic hybrid model of a linear, flexible, and elastic bead-spring polymer chain, consisting of $N = 30$ monomers, interacting with a cylindrical substrate. The interaction between pairs (i,j) of monomers of the polymer is described by a modified Lennard-Jones (LJ) potential

$$U_{\mathrm{LJ}}^{\mathrm{mod}}(r_{ij}) = \begin{cases} U_{\mathrm{LJ}}(r_{ij}) - U_{\mathrm{LJ}}(r_{\mathrm{c}}), & r_{ij} < r_{\mathrm{c}}, \\ 0, & \text{otherwise}, \end{cases} \quad (1)$$

where the standard LJ potential

$$U_{\mathrm{LJ}}(r_{ij}) = 4\varepsilon\left[\left(\frac{\sigma}{r_{ij}}\right)^{12} - \left(\frac{\sigma}{r_{ij}}\right)^{6}\right], \quad (2)$$

is truncated if the distance between the monomers r_{ij} exceeds the cut-off threshold $r_{\mathrm{c}} = 2.5\sigma$, and it is shifted by $U_{\mathrm{LJ}}(r_{\mathrm{c}})$ as to

[a] *Soft Matter Systems Research Group, Center for Simulational Physics, The University of Georgia, Athens, GA 30602, USA. E-mail: bachmann@smsyslab.org; Web: http://www.smsyslab.org*
[b] *Institut für Theoretische Physik and Centre for Theoretical Sciences (NTZ), Universität Leipzig, Postfach 100 920, D-04009 Leipzig, Germany. E-mail: gross@itp.uni-leipzig.de*
[c] *Department of Physics, Stetson University, DeLand, FL 32723, USA*
[d] *Theoretical Division, Los Alamos National Laboratory, Los Alamos, NM 87545, USA. E-mail: tvogel@lanl.gov*
[e] *Instituto de Física, Universidade Federal de Mato Grosso, 78060-900 Cuiabá, Mato Grosso, Brazil*
[f] *Departamento de Física, Universidade Federal de Minas Gerais, 31270-901 Belo Horizonte, Minas Gerais, Brazil*

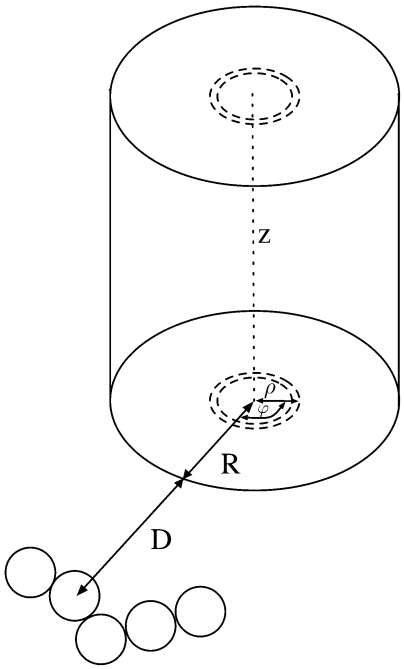

Fig. 1 Coordinates for integration of the Lennard-Jones potential in case of the nanocylinder.

prevent a discontinuity at $r = r_c$. In the simulations, the parameters were set to $\varepsilon = 1$, $\sigma = 2^{-1/6} r_0$, and $r_0 = 0.7$. The bond fluctuation width between bonded monomers is regularized by the finitely extensible nonlinear elastic (FENE) potential[29–31]

$$U_{\mathrm{FENE}}(r_{ii+1}) = -\frac{K}{2} l^2 \log\left[1 - \left(\frac{r_{ii+1} - r_0}{l}\right)^2\right]. \qquad (3)$$

Minimum potential positions of the FENE and LJ potentials coincide; the FENE potential diverges for $r \to r_0 \pm l$ and $l = 0.3$ was chosen. The FENE energy scale was adjusted by setting $K = 40$.

For the interaction of each monomer with the cylindrical substrate we assume that the distribution of matter in the cylinder is uniform. The integration of a standard LJ potential between a monomer, located at the distance D from the surface of the nanocylinder with radius R (see Fig. 1 for illustration), and a volume element of the cylinder yields:[15]

$$U_{\mathrm{cyl},R,\varepsilon_c}(D) = \varepsilon_c \pi \int_0^{2\pi} \mathrm{d}\varphi \int_0^R \rho \,\mathrm{d}\rho \left(\frac{63}{64 s^{11/2}} - \frac{3}{2 s^{5/2}}\right), \qquad (4)$$

with

$$s = (D + R)^2 + \rho^2 - 2\rho(D + R)\cos\varphi. \qquad (5)$$

The integration along the cylinder axis in z direction has already been performed. Different values of the adsorption strength parameter ε_c correspond to different nanocylinder materials.

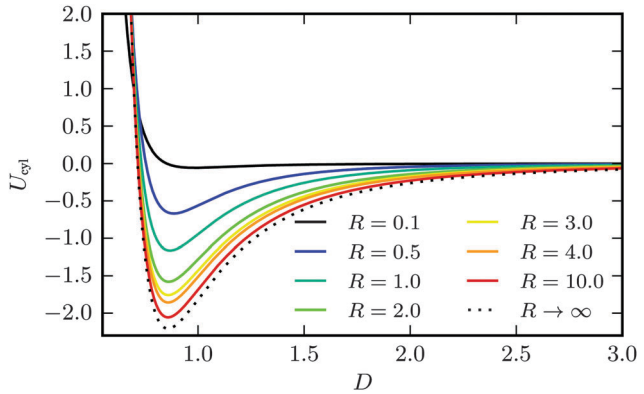

Fig. 2 Cylinder potential (4) for $\varepsilon_c = 1.0$ and different nanocylinder radii R. The dotted line represents the potential for $R \to \infty$, which coincides with the potential of a substrate with planar surface.

For computational reasons, we use in our simulations a modified version of this potential:

$$U^{\mathrm{mod}}_{\mathrm{cyl},R,\varepsilon_c}(D) = \begin{cases} \infty, & 0 \le D \le 0.5, \\ U_{\mathrm{cyl},R,\varepsilon_c}(D), & 0.5 < D < 5.0, \\ 0 & D > 5.0. \end{cases} \qquad (6)$$

In order to avoid the computationally intensive calculation of the integral in eqn (4) at each Monte Carlo step during the simulation, the cylinder potential was discretized and tabulated prior to the simulation and stored in memory.

For $\varepsilon_c = 1.0$, the cylinder potential is plotted in Fig. 2 at different values of the cylinder radius R. In the limiting case $R \to \infty$, the cylinder potential coincides with the potential of a three-dimensional substrate with planar surface. In this case, the integration of the Lennard-Jones potential over the half-space that is occupied by the substrate yields:[11,28]

$$U_{\mathrm{plan},\varepsilon_c}(D) = 4\pi\varepsilon_c \left(\frac{1}{45 D^9} - \frac{1}{6 D^3}\right). \qquad (7)$$

This allows a qualitative comparison of adsorbed structures at cylindrical substrates with results from previous studies of polymer adsorption at planar surfaces.[11,13,14]

For a given polymer conformation, represented by the coordinate vector of N monomers $\mathbf{X} = (\vec{r}_1, \ldots, \vec{r}_N)$ and interacting with a nanocylinder with radius R, the total energy is given by

$$E_{R,\varepsilon_c}(\mathbf{X}) = \frac{1}{2} \sum_{\substack{i,j=1 \\ i \neq j}}^{N} U^{\mathrm{mod}}_{\mathrm{LJ}}(r_{ij}) + \sum_{i=1}^{N-1} U_{\mathrm{FENE}}(r_{ii+1}) + \sum_{i=1}^{N} U^{\mathrm{mod}}_{\mathrm{cyl},R,\varepsilon_c}(D_i). \qquad (8)$$

Simulations were performed in a simulation box with steric walls in x and y direction. The size of the box in these directions was set to $R + 2N$. This restriction keeps the polymer from moving too far away from the cylinder. A limitation in z direction was not necessary, since the cylinder extends over the whole z axis. Simulations were performed using parallel tempering[32–35] at 112 temperatures in the interval $T \in [0.1, 2.5]$ for 5 different nanocylinder materials with $\varepsilon_c = \{1.0, 2.0, 3.0, 4.0, 5.0\}$ and 10 different radii

$R = \{0.1, 0.25, 0.5, 0.75, 1.0, 1.5, 2.0, 3.0, 4.0, 10.0\}$. For each temperature T, cylinder adsorption strength ε_c, and radius R, 5×10^7 Monte Carlo sweeps were performed to accumulate sufficient statistics for the analysis of canonical quantities. Error bars were obtained using the jackknife binning method.[28,36–38]

III Statistical analysis of polymer adsorption at nanocylinders

In this section, we discuss thermodynamic properties of energetic and structural quantities of a 30mer for various adsorption strengths and cylinder radii and identify temperatures at which pronounced thermal activity is observed. On this basis, we then construct hyperphase diagrams for the polymer parameterized by the temperature and material properties of the cylinder (adsorption strength, radius) in the following section.

For the analysis of macroscopic states and the identification of structural phases it is useful to investigate the response of relevant thermodynamic quantities to thermal effects. In canonical statistical analysis, the expectation value of an observable quantity $\mathcal{O}$ is defined by

$$\langle \mathcal{O} \rangle (T; R, \varepsilon_c) = \frac{1}{Z(T; R, \varepsilon_c)} \int \mathcal{D}X \mathcal{O}(\mathbf{X}) \mathrm{e}^{-E_{R,\varepsilon_c}(\mathbf{X})/k_B T}, \qquad (9)$$

where $\mathcal{D}X$ is the formal integration measure for the phase space of polymer conformations and

$$Z(T; R, \varepsilon_c) = \int \mathcal{D}X \mathrm{e}^{-E_{R,\varepsilon_c}(\mathbf{X})/k_B T}, \qquad (10)$$

is the canonical partition function of the polymer interacting with a cylinder whose material properties are characterized by adsorption strength ε_c and radius R. Fluctuations of $\mathcal{O}$ can suitably be defined by the temperature derivative of the mean,

$$\frac{\mathrm{d}\langle \mathcal{O} \rangle}{\mathrm{d}T} = \frac{1}{k_B T^2} (\langle \mathcal{O} E \rangle - \langle \mathcal{O} \rangle \langle E \rangle). \qquad (11)$$

Extremal fluctuations help locate and identify structural transitions of the polymer.

A Energetic fluctuations: specific heat

The most natural quantity and also the most general "order" parameter to take a first look at is the mean energy $\langle E_{R,\varepsilon_c} \rangle$. Its fluctuation is associated with the specific heat of the system $c_V = (1/N)\mathrm{d}\langle E_{R,\varepsilon_c} \rangle / \mathrm{d}T$. Fig. 3 shows the specific-heat plots for various cylinder radii R and adsorption strengths ε_c. For $\varepsilon_c = 1.0$, the curves exhibit two peaks for most radii. The stable peak position for all radii at $T \approx 0.35$ signals the freezing or liquid–solid transition of desorbed and adsorbed polymer structures, respectively. Below that temperature all polymers, adsorbed or desorbed, have a well defined crystalline structure. For $R = 10.0$ the freezing temperature is slightly shifted to a lower temperature. The reason for this becomes apparent later, when we investigate the structural properties of the crystalline phase in more detail.

The second peak at higher temperatures, visible for all radii $R > 0.25$, signals the adsorption transition. In this case, the adsorption point is shifted to higher temperatures with increasing cylinder radius. For larger adsorption strengths, also shown in Fig. 3, the specific-heat curves exhibit more pronounced features at temperatures below $T = 1.5$ that indicate additional transitions. Their interpretation requires the analysis of more specific order parameters.

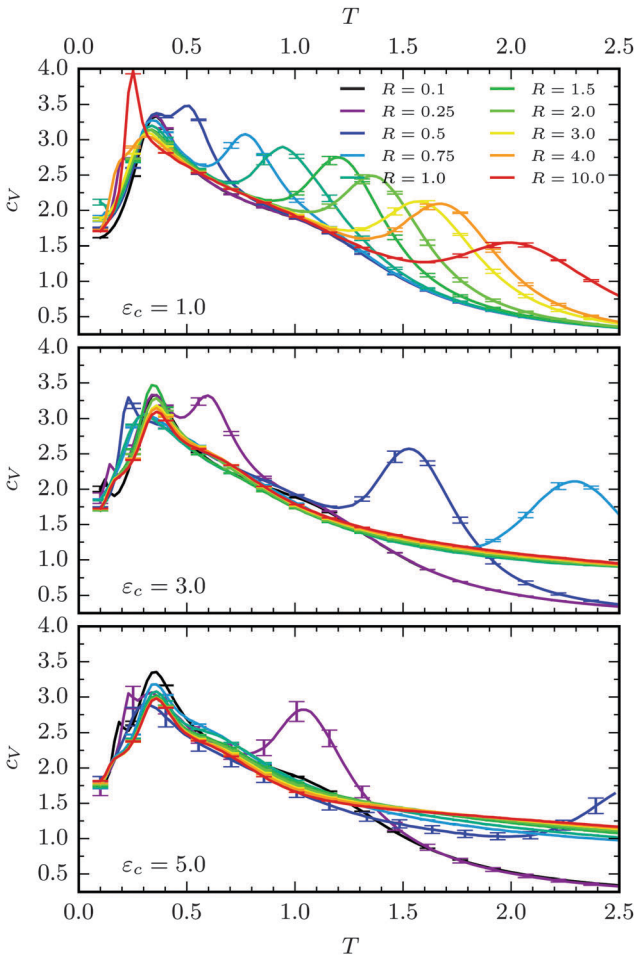

Fig. 3 Specific-heat curves for the interaction of a 30mer with nanocylinders at 10 different radii $R \in [0.1, 10.0]$, plotted for adsorption strengths $\varepsilon_c = 1.0$, 3.0, and 5.0.

B Order parameters and their thermal fluctuations

The canonical average of the squared radius of gyration, $\langle r_{\mathrm{gyr}}{}^2 \rangle = \sum_{i=1}^{N} \left\langle (\vec{r}_i - \vec{r}_{\mathrm{cm}})^2 \right\rangle \Big/ N$, where $\vec{r}_{\mathrm{cm}} = \sum_{i=1}^{N} \vec{r}_i / N$ is the center of mass of the polymer, is a measure for the compactness of a polymer conformation. For this reason, it has been used as a particularly useful quantity for the analysis of the critical behavior near the collapse transition.

In Fig. 4(left panel), the squared radius of gyration is plotted as a function of temperature for various cylinder radii and the adsorption strengths $\varepsilon_c = 1$, 3, and 5. The fluctuations of this quantity, $\mathrm{d}\langle r_{\mathrm{gyr}}{}^2 \rangle / \mathrm{d}T$, are depicted in the right panel of the same figure. These plots reveal a number of distinct features associated with the cooperativity or competition of adsorption and structure

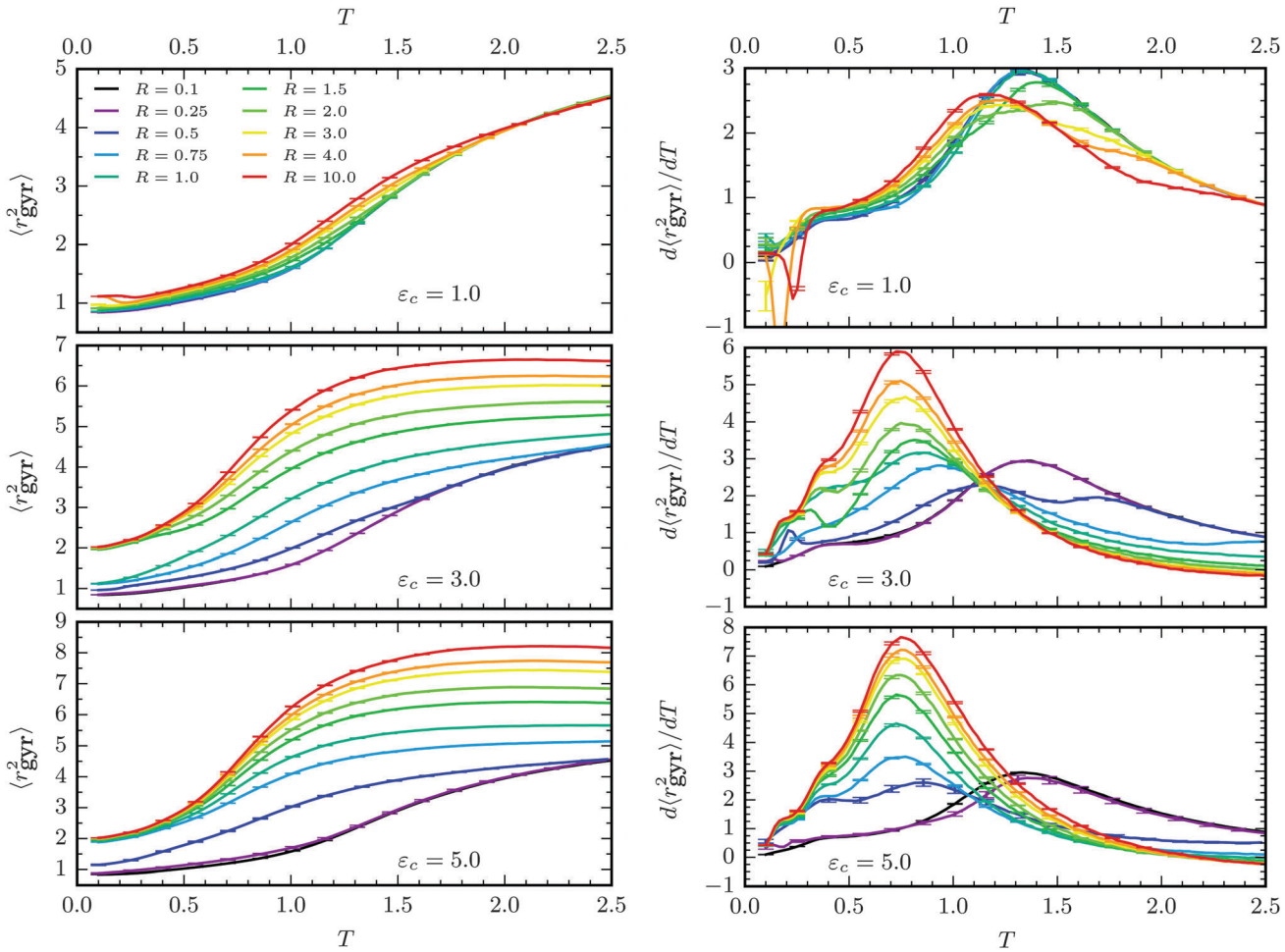

Fig. 4 Mean squared radius of gyration and its fluctuation as a function of temperature for the 30mer for various cylinders radii and different values of the adsorption strength ε_c.

formation and the dependency of these processes on the system parameters. It is important to note that the physical meaning of transition signals like peaks or "shoulders" that lie close to each other for different cylinder radii and adsorption strengths can be different and depends on the precise values of these system parameters.

The radius of gyration fluctuates the most if the polymer structure experiences a significant change in its overall extension. Therefore, $d\langle r_{gyr}{}^2\rangle/dT$ is useful for the identification of the transition between random-coil structures ("gas phase") and globular conformations ("liquid phase"), independently of whether the polymer is adsorbed or desorbed.

To verify whether the polymer is adsorbed at the surface, we introduce the number of surface contacts n_c. A monomer is considered to be in contact with the nanocylinder if its distance from the cylinder surface is $D \leq 0.95$, which is slightly above the distance of minimal cylinder potential. In Fig. 5, the average number of surface contacts $\langle n_c \rangle$ (left panel) and its thermal fluctuation $d\langle n_c \rangle/dT$ (right panel) is plotted as a function of temperature for all simulated values of R and ε_c. The number of contacts provides also insight into structural features in the low-temperature phases and lowest-energy states.

Eventually, we have also measured the perpendicular distance of the center of mass of the polymer from the cylinder surface, $r_\perp$, which offers additional structural information in the low-temperature and in the adsorption/desorption regimes. The canonical averages and the fluctuations about the mean are plotted in Fig. 6.

These quantities form a set of order parameters that is helpful for identifying and interpreting the structural transitions of the polymer.

For $\varepsilon_c = 1$, we find particularly pronounced coil-globule transition signals in the radius of gyration curves [Fig. 4(top)] at temperatures $T > 1$ for all cylinder radii. However, these signals indicate different scenarios, which becomes obvious when comparing with Fig. 5(top). If the cylinder radius is smaller than $R = 1.5$, there is only one peak at about $T = 1.35$. In this case, the polymer is desorbed ($\langle n_c \rangle \approx 0$) and experiences the typical Θ collapse transition in free space between desorbed-expanded structures (DE) and desorbed-globular structures (DG). For larger radii, $R > 1.5$, however, the behavior is more interesting. The transition signal splits into two. The signal at lower temperature indicates the collapse transition of the polymer while it is in contact with the cylinder, between

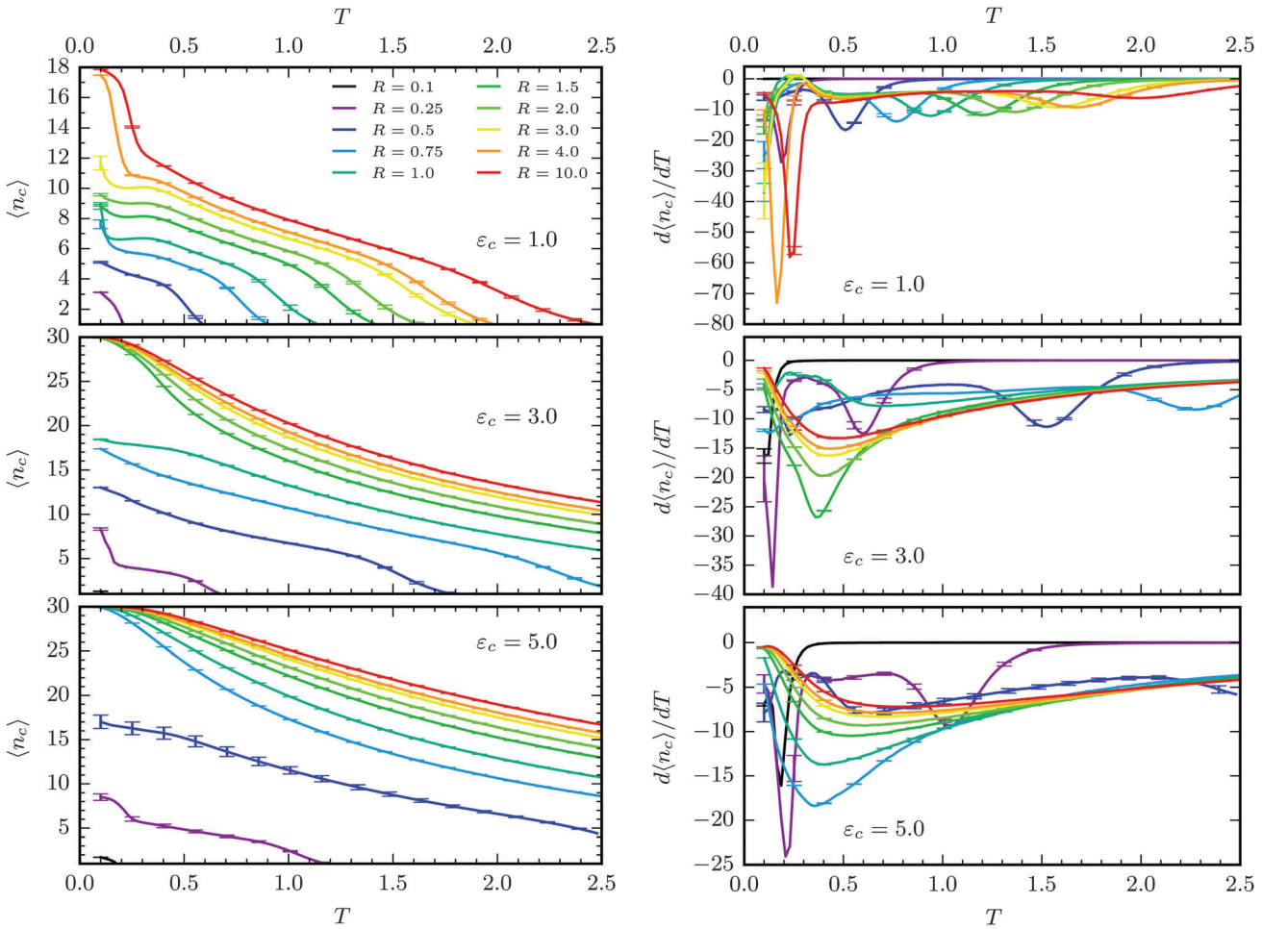

Fig. 5 Temperature dependence of the mean number of surface contacts (and fluctuations) of a 30mer with nanocylinders of different radii for three adsorption strengths.

adsorbed-globular (AG) and adsorbed-expanded conformations (AE). The number of surface contacts is nonzero and does not exhibit a significant change.

The other transition signal at higher temperatures ($T > 1.4$) is caused by the different conformational entropies of cylinder-adsorbed polymer structures and entirely desorbed conformations. While the radius of gyration does not account for changes in the translational entropy, $\langle r_\perp \rangle$ [Fig. 6(top)] does and possesses clear peaks indicating the adsorption transition between AE and DE conformations. Consequently, the number of surface contacts drops rapidly upon passing the transition by increasing the temperature.

The low-temperature transition behavior is way more complex and depends sensitively on the cylinder radius. If the radius is very small ($R < 0.25$), the number of possible monomer–surface contacts is extremely limited such that for $\varepsilon_c = 1.0$ the polymer effectively ignores the presence of the substrate and remains desorbed most of the time. This is also the case at very low temperatures, where the polymer structures are desorbed-compact (DC).

For slightly larger radii, the polymer recognizes the cylinder substrate in a well-defined way. Below $R = 0.5$, the polymer conformation remains most compact, the number of surface contacts is nonzero but small (which means the polymer is adsorbed), and the distance of the center of mass relatively large for an adsorbed structure. This means the polymer binds to the cylinder as an adsorbed-compact droplet (ACD). Upon increasing the cylinder radius, *i.e.*, for less curved surfaces, the polymer forms more regular adsorbed-compact structures with three layers (AC3) and about 8 to 12 surface contacts; for radii $R > 3.5$ double-layers (AC2) with about 18 contacts in the surface layer become energetically favorable. It is worth noting that the surface attraction is too weak to allow for single-layered (filmlike) structures.

If the cylinder attraction strength is increased to $\varepsilon_c = 3.0$, several significant changes in the polymer adsorption behavior can be noticed. As expected, the adsorption transitions shift to much higher temperatures. For example, if the cylinder radius is chosen to be $R = 0.5$, the adsorption temperature changes from $T \approx 0.5$ at $\varepsilon_c = 1.0$ to $T \approx 1.5$ at $\varepsilon_c = 3.0$, as can be seen easily when comparing Fig. 5(top right) and Fig. 5(center right).

Another interesting feature is that, while the Θ transition of the "free" polymers is obviously scarcely affected, the confined Θ transition of the adsorbed polymers on the surface (AG/AE) shifts to lower temperatures. This is clearly visible in the corresponding curves for the fluctuations of the radius of gyration in Fig. 4(center right). Toward larger radii, the AG/AE transition

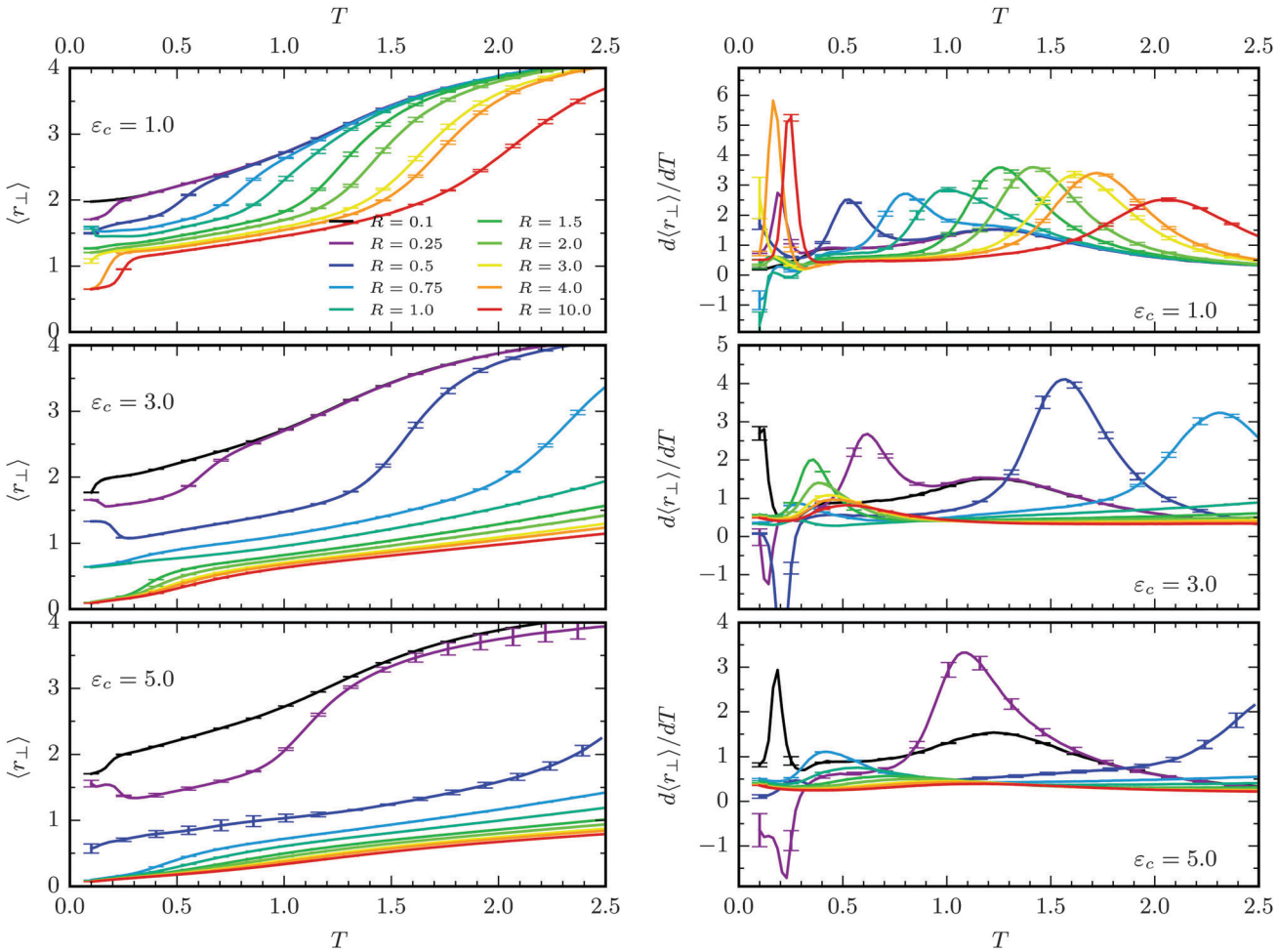

Fig. 6 Mean perpendicular (radial) distance of the center of mass of the polymer from the cylinder surface, $\langle r_\perp \rangle$, and its fluctuation $d\langle r_\perp \rangle/dT$ as a function of temperature for the 30mer for different cylinder parameters.

temperature converges to about $T = 0.75$ for $R = 10$ (as compared to $T \approx 1.2$ at $\varepsilon_c = 1.0$). The fact that adsorption occurs at higher and the collapse into globular structures at lower temperatures suggests that higher adsorption strengths quench the polymer and make it bind to the substrate in entropically reduced and rather "flat" adsorbed structures (AE) that prevent the monomers to assemble in more ordered arrangement. Consequently, a stronger adsorption strength effectively suppresses the formation of compact unit cells of monomers as competing surface-monomer contacts become favorable as well. The smaller extension of adsorbed polymer structures in the directions perpendicular to the surface of the substrate is obvious when comparing the corresponding $\langle r_\perp \rangle$ curves in Fig. 6 at $\varepsilon_c = 1.0$ and 3.0 for radii $R > 1$.

Despite this increased preference of disordered adsorbed structures below the transition point, it is one of the most remarkable features of all order parameter curves at $\varepsilon_c = 3.0$ (and higher) that the recognition of the cylinder geometry by the polymer already occurs in the AE phase. The curves tend to group, and these groups ultimately embark into the formation channels of distinct and unique compact adsorbed structures at very low temperatures. In this lowest-temperature regime, the most noteworthy changes compared to the $\varepsilon_c = 1$ case are the suppression of DC structures in favor of an extended phase of adsorbed compact conformations (ACD), and the appearance of a dominant compact monolayer phase (AC1). The filmlike monolayer is maximally compact and all monomers are in contact with the substrate. It is topologically two-dimensional. This is important to note because at the adsorption strength considered here ($\varepsilon_c = 3$), the polymer has to undergo a topological transition to reach the globular phase AG, *i.e.*, overcoming the surface tension and forming a three-dimensional globular structure by increasing the temperature only is a cooperative one-step process. This rather unusual highly cooperative behavior cannot be expected to prevail for larger adsorption strengths.

Indeed, for $\varepsilon_c = 5$, we find that additional phases emerge. The melting of the AC1 structures for radii $R > 0.6$ results in the formation of two-dimensional monolayer, but not filmlike, "globular" polymer conformations. Upon further increasing the temperature, the contacts between the monomers are released, but the monomers remain bound to the substrate. For radii $R > 1.5$, the adsorbed-expanded structures are still essentially two-dimensional (AE1), before additional heating allows the now isolated monomers to lift off the substrate and enter phase AE by experiencing a topological transition. The signature of

this rather weak transition is found in the fluctuations of $r_\perp$ shown in Fig. 6(bottom right).

IV Hyperphase diagrams

The careful extraction of the information gathered from the analysis of the specific-heat curves and the fluctuations of the order parameters enables us to construct and compare the hyperphase diagrams for the hybrid system of the 30mer and nanocylinder. For the cylinder adsorption strengths ε_c = 1.0, 3.0, and 5.0, the structural phase diagrams in T–R space are shown in Fig. 7. Transition lines were obtained by connecting transition points associated with signals of extremal thermal activity (peaks, ''shoulders'') in the fluctuations of the thermodynamic quantities discussed in the previous section. Since the polymer system is finite, the estimated transition temperatures typically depend on the choice of the thermodynamic quantity. This ambiguity is inherent to the conventional canonical statistical analysis we perform here. The associated uncertainty in the location of transition points has been accounted for by drawing transition bands rather than lines.

Since in our study the polymer is not grafted on the cylinder surface, the hyperphase diagrams consist of two clearly separated main parts: the phases of desorbed and adsorbed polymer conformations. The desorbed phases dominate for hybrid systems, in which the cylinder radius is small and the surface attraction weak. The polymer recognizes the energetic advantage of binding to the cylinder only at lowest temperatures, where entropy is less relevant. Thus, in the desorbed phases, the structural transition behavior of the polymer is virtually the same as if it resides in unconfined free space. The structural phases in this region are the random coils (DE), the more compact but only locally ordered globular structures (DG), and the crystalline compact conformations (DC). The transition between DE and DG is the well-studied Θ collapse transition, but also progress in understanding the liquid–solid transition DG $\Leftrightarrow$ DC better has been made recently.[39–41] Representative examples are shown in Fig. 8.

Well separated from the desorbed phases by the strong adsorption transition line, the adsorbed phases can roughly be distinguished in a similar way (AE, AG, AC), but local details matter and, therefore, it is necessary to subdivide these phases into local regimes. In this context it is also useful to recap that in the limit of vanishing radius, the nanocylinder exhibits features of a nanowire. The interaction of a flexible polymer with a nanowire has been studied recently.[19–21,24] In the opposite limit of very large radii, the local curvature of the cylinder becomes negligible and the polymer adsorption behavior is identical to that near a perfectly flat substrate.[11] Our study interpolates between these two limits.

In the adsorbed-expanded phase AE, which dominates the adsorption behavior at high temperatures, the polymer attaches to the cylinder in an unspecified way. The polymer structure is basically randomly extending into three dimensions and contacts to the surface are loose. While the polymer recognizes the energetic gain of binding to the substrate, it still takes advantage of large

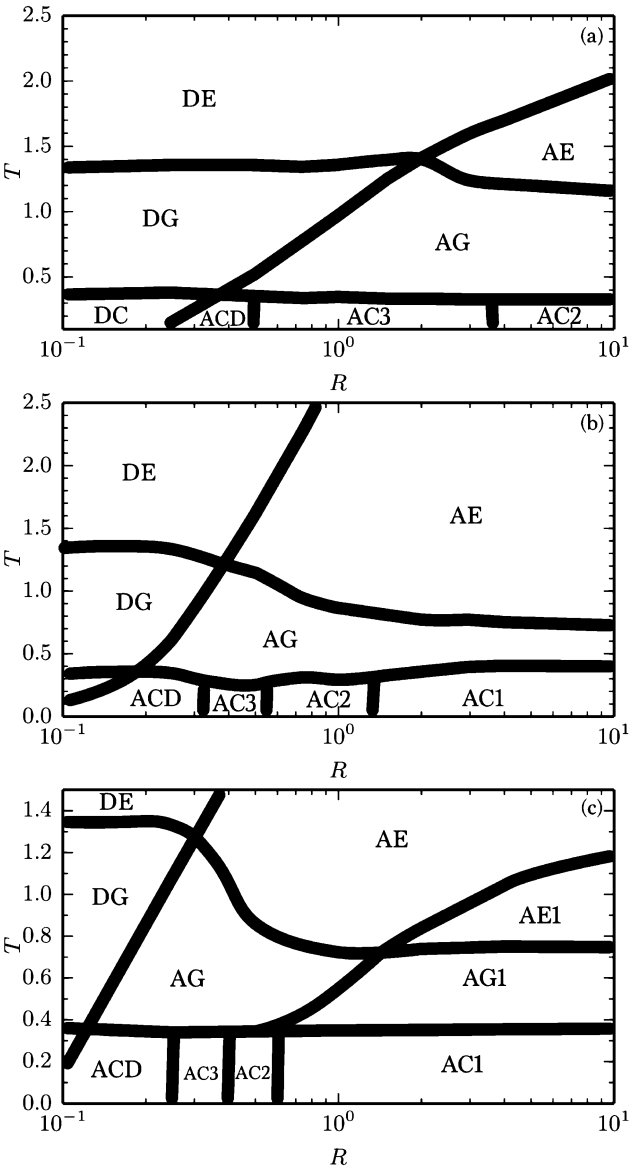

Fig. 7 Hyperphase diagram of the 30mer in the space of cylinder radii R and temperature T for cylinder adsorption strengths (a) ε_c = 1.0, (b) ε_c = 3.0, and (c) ε_c = 5.0. Note the different temperature scale in (c).

conformation-entropic freedom, but substantially loses translational entropy. This loss of translational entropy is the only reason why the adsorption transitions (DE $\Leftrightarrow$ AE, DG $\Leftrightarrow$ AG, DC $\Leftrightarrow$ ACD) of the nongrafted, finite polymer are discontinuous (first-order-like).[13] However, it should be noted that the adsorption transition becomes continuous in the thermodynamic limit.[1]

We would like to emphasize that the location of the adsorption transition depends also on the monomer concentration. Translational entropy effects influence the adsorption behavior and are stronger in the dilute regime. However, as it has been shown recently,[13] the finite-size effects of system and environment at constant concentration N/V, where N is the chain length and V is the accessible volume of the simulation box, are minor.

In Fig. 9, we have plotted for ε_c = 3.0 and R = 0.5 the free energies of the adsorbed and the desorbed states (up to an irrelevant

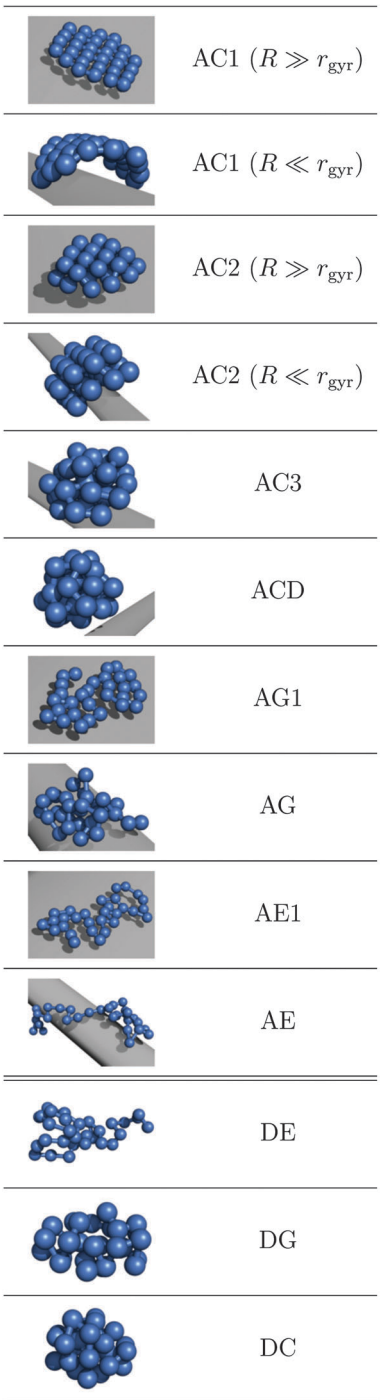

Fig. 8 Characteristic conformations in the structural phases of a 30mer interacting with a nanocylinder.

contribution $F_0(T) = -TS_0$ due to the unknown absolute entropy shift S_0),

$$F_{ads,des}(T) - F_0(T) = -k_B T \ln Z_{ads,des}(T), \qquad (12)$$

as functions of temperature T. The respective partition functions are given by $Z_{ads}(T) = \int_{E_0}^{E_{sep}} g(E) \exp(-E/k_B T)$ and $Z_{des}(T) = \int_{E_{sep}}^{\infty} g(E) \exp(-E/k_B T)$. Here, $g(E)$ is the density of states, E_0 is the ground state energy, and E_{sep} is the energy at the separation point between the peaks of the equal-weight bimodal energy distribution. We have also included the minimum free energy curve in Fig. 9 (dashed line), which exhibits a kink at the crossover point between adsorbed and desorbed phases. The temperature at the kink location coincides with the transition point in the phase diagram Fig. 7(b), indicating that the adsorption–desorption transition is first-order-like.

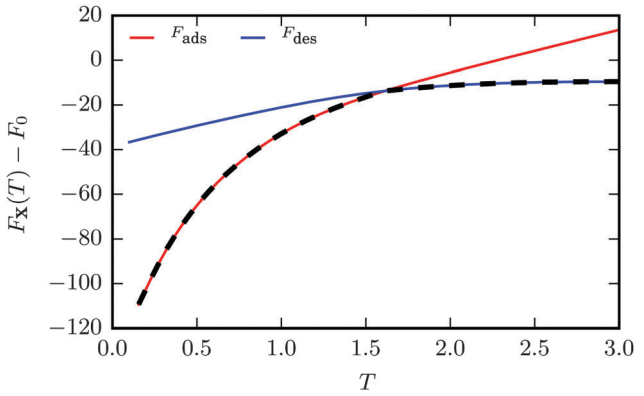

Fig. 9 Free energies of adsorption and desorption, F_{ads} and F_{des} for the 30mer at $\varepsilon_c = 3.0$ and $R = 0.5$ as a function of the temperature T. The dashed line represents the minimum free energy and clearly shows a kink at the transition point, indicating that under these conditions for the nongrafted, finite system the adsorption–desorption transition is first-order-like.

The adsorbed-globular phase AG is dominated by disordered, liquid-like conformations. While local ordering of contacts sets in, no obvious long-range order on scales beyond nearest-neighbor contacts emerges. In the intermediate temperature region, in which this phase is located in the phase diagram, conformational entropy is reduced further, and the energetically preferred formation of surface contacts renders substrate binding stronger than in AE.

The most remarkable transition is associated with the crystallization of the polymer on the substrate if the system is cooled down below the freezing transition temperature. Although the solid phases differ and the solid–solid transitions among them relocate in R space upon changing the surface attraction strength ε_c, we did not find significant changes in the transition behavior from the liquid into the solid phases. In particular, the transition temperature is very stable at about $T = 0.35$, independently of the cylinder properties. This means that the geometric ordering of the monomers is not induced or influenced by the surface; it is an inherent intra-monomeric process of the polymer. Taking into account that at a given cylinder radius R the type of the solid phase into which the polymer crystallizes depends on the surface attraction strength, one may conclude that the relevant phase space of geometric polymer structures in the disordered phases, limited by the system's energetic scales, already determines the transition pathways into the solid phases. A careful analysis of this hypothesis is worth a future study, but exceeds the scope of this paper.

The specific features of the solid phases depend on the cylinder geometry and the energy scale of attraction. For very

small radii, the optimal adsorbed energetic state of the polymer is a structure that resembles the DC ground state: compact, with smallest surface, and only locally attached to the nanocylinder. We call these conformations adsorbed-compact droplets (ACD). The more global recognition of the substrate at larger cylinder radii leads to a rearranged monomer configuration and the condensed droplets possess a more ordered internal structure. Consequently, layered structures are formed, starting with a triple-layer conformation (AC3). By increasing the cylinder radius, the polymer is wetting the surface. Double-layer structures in phase AC2 are finally followed by monolayer films (AC1), provided the surface attraction strength of the cylinder substrate is large enough. The layered conformations can be bent and wrap around the substrate. Because of the limited system size, complete embracement of the cylinder was not observed, but is possible for sufficiently long chains. Such polymer tubes have been found in recent adsorption studies on nanowires.[19–21,24]

For increasingly large surface attraction strengths ε_c, the monolayer phase becomes more and more dominant, *i.e.*, wetting the surface out of the AE/AG phases is the major adsorption process. However, the strong affinity of individual monomer adsorption even at relatively high temperatures paired with the demand to crystallize in a monolayer (which causes the polymer to experience a topological transition) requires such a high cooperativity that the AG and AE phases degenerate and additional subphases form [*e.g.*, for $\varepsilon_c = 5.0$ as shown in Fig. 7(c)]. For sufficiently flat substrates, the system undergoes the topological transition from expanded three-dimensional states (AE) to two-dimensional conformations (AE1) without any ordering. Effectively, each monomer binds individually, non-cooperatively to the substrate. Then local ordering occurs in phase AG1. The transition AE1 $\Leftrightarrow$ AG1 is remarkable, because it is a two-dimensional variant of the Θ collapse transition. Eventually, the local clusters bind to each other and form a compact, crystalline monolayer (AC1).

V Summary and perspectives

In this paper, we have investigated the thermodynamic adsorption behavior of a flexible homopolymer near an attractive cylindrical surface. In extensive replica-exchange simulations of a generic coarse-grained model for the hybrid polymer–cylinder system, we systematically examined the influence of the cylinder radius and attraction strength upon the cooperative effects that enable the formation of adsorbed polymer conformations. For the identification and investigation of the structural phases of the polymer, we performed a comprising conventional canonical statistical analysis of the thermal fluctuations of energy and appropriate order parameters (such as radius of gyration, number of surface contacts, and perpendicular distance of the polymer center of mass from the cylinder surface).

For this purpose, we studied the response of the order parameters to changes of the temperature for various system parameter settings (cylinder radius and adsorption strength). Extremal fluctuations were interpreted as signals of advanced thermal activity of the system and used as indicators of structural transitions. The thus obtained transition points were used to construct complete structural phase diagrams for various adsorption scenarios. Effectively, we performed parameter scans in model (or material) space, which can only be done on the level of minimalistic generic models as employed in this study. Hence, the structural phase diagrams, parameterized by temperature and cylinder radius and fixed cylinder adsorption strength, are hyperphase diagrams.

The complexity of this study limited the system size to 30 monomers, but by exemplified comparisons with larger systems and previous studies of different substrates, we are confident that the major qualitative features of the hyperphase diagrams are representative. We would also like to emphasize that the extrapolation toward the thermodynamic limit was not in the focus of this study. Finite-size effects are essential for biological and nanotechnological function and need to be considered as integral part of any statistical analysis of functional soft matter on mesoscopic scales. This impacts, for example, the "crystalline" structure of compact conformations which typically do not possess specific long-range symmetries, because of significant surface effects.

Since on one hand a cylinder with vanishing radius mimics a nanowire and, on the other hand, a large radius entails a locally almost flat surface, our study interpolates between these two well-studied cases. The hyperphase diagrams clearly reveal the influence of the cylinder radius upon the formation of structural phases, in combination with its attraction strength. The adsorption processes from the desorbed phases into the compact, firmly bound adsorbed polymer conformations differ qualitatively when comparing systems with different cylinder geometries. Generally, increased surface attraction strengths favor the formation of monolayers, provided the energy scale is sufficiently large. However, the topological transition from three-dimensional expanded or globular conformations into two-dimensional structures requires high cooperativity. As our results show, if the surface attraction strength is too small compared to the internal attractive monomer–monomer interaction, topological transitions do not occur. For relative energy scales beyond a certain threshold, complexity dictates a cooperative adsorption process to pass through a topological transition that includes multiple steps.

To summarize, our study has shown that geometric and energetic parameters of cylindrical substrates influence the way polymers bind to such substrates. Despite the simplicity of nanocylinders, complex adsorption processes of polymers can be modified and made substrate-specific.[42] Therefore, the results of this study are potentially helpful for applications of hybrid systems composed of soft and solid matter, such as coating of nanotubes by polymers, that enable the manipulation of physical properties (*e.g.*, elasticity, conductivity) of curved substrates. The specificity of binding that we found makes cylindrical nanoparticles also interesting systems for nanosensing macromolecules in polymer solvents.[43]

Acknowledgements

This work has been supported partially by the NSF under Grant No. DMR-1207437, by CNPq (National Council for Scientific

and Technological Development, Brazil) under Grant No. 402091/2012-4, and by the DFG (German Research Foundation) under Grant No. SFB/TRR 102 (Project No. B04). Assigned LA-UR-15-25031.

References

1 E. Eisenriegler, K. Kremer and K. Binder, *J. Chem. Phys.*, 1982, **77**, 6296.
2 T. Vrbová and S. G. Whittington, *J. Phys. A: Math. Gen.*, 1996, **29**, 6253.
3 T. Vrbová and S. G. Whittington, *J. Phys. A: Math. Gen.*, 1998, **31**, 3989.
4 T. Vrbová and K. Procházka, *J. Phys. A: Math. Gen.*, 1999, **32**, 5469.
5 A. Milchev and K. Binder, *J. Chem. Phys.*, 2001, **114**, 8610.
6 Y. Singh, D. Giri and S. Kumar, *J. Phys. A: Math. Gen.*, 2001, **34**, L67.
7 R. Rajesh, D. Dhar, D. Giri, S. Kumar and Y. Singh, *Phys. Rev. E: Stat., Nonlinear, Soft Matter Phys.*, 2002, **65**, 056124.
8 J. Krawczyk, A. L. Owczarek, T. Prellberg and A. Rechnitzer, *Europhys. Lett.*, 2005, **70**, 726.
9 M. Bachmann and W. Janke, *Phys. Rev. Lett.*, 2005, **95**, 058102.
10 M. Bachmann and W. Janke, *Phys. Rev. E: Stat., Nonlinear, Soft Matter Phys.*, 2006, **73**, 041802.
11 M. Möddel, M. Bachmann and W. Janke, *J. Phys. Chem. B*, 2009, **113**, 3314.
12 L. Wang, T. Chen, X. Lin, Y. Liu and H. Liang, *J. Chem. Phys.*, 2009, **131**, 244902.
13 M. Möddel, W. Janke and M. Bachmann, *Phys. Chem. Chem. Phys.*, 2010, **12**, 11548.
14 M. Möddel, W. Janke and M. Bachmann, *Macromolecules*, 2011, **44**, 9013.
15 A. Milchev and K. Binder, *J. Chem. Phys.*, 2002, **117**, 6852.
16 I. Gurevitch and S. Srebnik, *Chem. Phys. Lett.*, 2007, **444**, 96.
17 I. Gurevitch and S. Srebnik, *J. Chem. Phys.*, 2008, **128**, 144901.
18 S. Srebnik, *J. Polym. Sci., Part B: Polym. Phys.*, 2008, **46**, 2711.
19 T. Vogel and M. Bachmann, *Phys. Rev. Lett.*, 2010, **104**, 198302.
20 T. Vogel and M. Bachmann, *Phys. Procedia*, 2010, **4**, 161.
21 T. Vogel and M. Bachmann, *Comput. Phys. Commun.*, 2011, **182**, 1928.
22 T. Vogel, T. Mutat, J. Adler and M. Bachmann, *Commun. Comput. Phys.*, 2013, **13**, 1245.
23 S. Karalus, W. Janke and M. Bachmann, *Phys. Rev. E: Stat., Nonlinear, Soft Matter Phys.*, 2011, **84**, 031803.
24 T. Vogel, J. Gross and M. Bachmann, *J. Chem. Phys.*, 2015, **142**, 104901.
25 A. G. Cherstvy and R. G. Winkler, *Phys. Chem. Chem. Phys.*, 2011, **13**, 11686.
26 D. Zhang, *et al.*, *J. Phys. Chem. B*, 2011, **115**, 14333.
27 S. J. de Carvalho, R. Metzler and A. G. Cherstvy, *Soft Matter*, 2015, **11**, 4430.
28 M. Bachmann, *Thermodynamics and Statistical Mechanics of Macromolecular Systems*, Cambridge University Press, Cambridge, 2014.
29 R. B. Bird, C. F. Curtiss, R. C. Armstrong and O. Hassager, *Dynamics of Polymeric Liquids*, Wiley, New York, 2nd edn, 1987.
30 K. Kremer and G. S. Grest, *J. Chem. Phys.*, 1990, **92**, 5057.
31 A. Milchev, A. Bhattacharaya and K. Binder, *Macromolecules*, 2001, **34**, 1881.
32 R. H. Swendsen and J.-S. Wang, *Phys. Rev. Lett.*, 1986, **57**, 2607.
33 K. Hukushima and K. Nemoto, *J. Phys. Soc. Jpn.*, 1996, **65**, 1604.
34 K. Hukushima, H. Takayama and K. Nemoto, *Int. J. Mod. Phys. C*, 1996, **7**, 337.
35 C. J. Geyer, in *Computing Science and Statistics*, Proceedings of the 23rd Symposium on the Interface, ed. by E. M. Keramidas, Interface Foundation, Fairfax Station, 1991, p. 156.
36 W. Janke, in *Proceedings of the Euro Winter School Quantum Simulations of Complex Many-Body Systems: From Theory to Algorithms, NIC Series*, ed. J. Grotendorst, D. Marx and A. Muramatsu, John von Neumann Institute for Computing, Jülich, 2002, vol. 10, p. 423.
37 D. P. Landau, *Phys. Rev. B: Solid State*, 1976, **13**, 2997.
38 W. W. Wood, *Physics of Simple Liquids*, Wiley, New York, 1968.
39 S. Schnabel, T. Vogel, M. Bachmann and W. Janke, *Chem. Phys. Lett.*, 2009, **476**, 201.
40 S. Schnabel, M. Bachmann and W. Janke, *J. Chem. Phys.*, 2009, **131**, 124904.
41 S. Schnabel, D. T. Seaton, D. P. Landau and M. Bachmann, *Phys. Rev. E: Stat., Nonlinear, Soft Matter Phys.*, 2011, **84**, 011127.
42 M. Q. Tran, J. T. Cabral, M. S. P. Shaffer and A. Bismarck, *Nano Lett.*, 2008, **8**, 2744.
43 M. Gao, L. Dai and G. G. Wallace, *Electroanalysis*, 2003, **15**, 1089.